

Multiple and Asymmetric Scalings in Explosive Percolation

Ming Li,^{1,*} Junfeng Wang,¹ and Youjin Deng^{2,3,†}

¹*Department of Physics, Hefei University of Technology, Hefei, Anhui 230009, P. R. China*

²*Hefei National Laboratory for Physical Sciences at Microscale and Department of Modern Physics, University of Science and Technology of China, Hefei, Anhui 230026, P. R. China*

³*MinJiang Collaborative Center for Theoretical Physics, Department of Physics and Electronic Information Engineering, Minjiang University, Fuzhou, Fujian 350108, P. R. China*

(Dated: August 23, 2022)

Explosive percolation in the Achlioptas process has recently attracted much research attention. From extensive simulations in an event-based ensemble, we find that, in dimensions from 2 to 6 and on random graphs, the Achlioptas processes all have two scaling windows and multiple fractal structures. The mixing of these multiple scalings successfully explains the previously observed anomalous phenomena in the conventional ensemble, and, moreover, correct critical exponents are now determined with a high precision by the event-based method. The multiple scalings and the ensemble inequivalence may bring new insights for other statistical systems.

Percolation is one of the paradigms in statistical physics and probability theory [1]. The standard percolation model on a lattice is defined by randomly occupying sites or bonds with an independent probability, and undergoes a continuous phase transition. A simple alteration of the percolation, such as lattice type, only results in a different critical point, and does not change the universality class [1]. By adopting significantly different percolation rules, such as rigidity percolation [2, 3], new universalities can arise. Further, by introducing the dimension of time, the directed percolation [4, 5] converts the percolation to a dynamical process and the transition becomes a non-equilibrium type with asymmetric exponents in spatial and temporal dimensions. Nevertheless, the continuity of the transition remains robust.

In recent years, there is an ongoing discussion on the so-called Achlioptas process [6], in which some intrinsic mechanism is introduced to suppress the growth of large clusters so that the percolation transition is delayed and becomes explosively sharp. A basic way is called the product rule [7]. At each time step, a random pair of empty bonds is picked up, the size product of the two clusters containing the ending sites of each bond is calculated, and the one, leading to a smaller size product, is inserted. As a consequence, the onset of percolation is significantly delayed, but once it happens, large clusters emerge suddenly, hence the name explosive percolation. A wide class of Achlioptas processes with explosive transition has been observed [6], including on regular lattices [8, 9] and scale-free networks [10, 11], and systems with other percolation rules [12–16].

Along with the sudden appearance of large clusters, the explosive percolation shows rich phenomena which are often recognized as signs of a discontinuous phase transition, such as the powder keg mechanism [12], bimodal distribution of the order parameter [17, 18], non-self-averaging property [16], and hysteresis [19]. Actually, the explosive percolation was perceived as a discontinuous transition when it was introduced [7–12, 14, 20, 21]. However, later studies suggested that the sharp transition is continuous, but exhibits anomalous critical behaviors [13, 17, 22–24]. A theoretical

study [23] rigorously proves that the explosive percolation is always a continuous transition unless a global dynamic is applied [25, 26]. It is now a common belief that the continuity is an essential feature of explosive percolation and of its variants [6]. However, the underlying mechanism for the anomalous phenomena, particularly those misinterpreted as signs of discontinuous transition, remains elusive, and a robust estimate of critical exponents is still challenging.

In this Letter, we perform a systematic and extensive simulation of the Achlioptas process in spatial dimensions from 2 to 6 and on random graphs. Given a finite system of sites N , we define the pseudo-critical point in each random dynamic process as the time step \mathcal{T}_N when the incremental size of the largest cluster reaches its maximum [15, 22, 27], and calculate its average $T_N \equiv \langle \mathcal{T}_N \rangle$ and variance $\sigma_{\mathcal{T}} \equiv \sqrt{\langle \mathcal{T}_N^2 \rangle - \langle \mathcal{T}_N \rangle^2}$. We observe two scaling windows: the distance of T_N to the thermodynamic percolation threshold T_c is $T_N - T_c \sim \mathcal{O}(N^{-1/\nu_1})$ and the variance is $\sigma_{\mathcal{T}} \sim \mathcal{O}(N^{-1/\nu_2})$, with exponent $\nu_2 > \nu_1$. This is dramatically different from the standard continuous transition, for which both $T_N - T_c$ and $\sigma_{\mathcal{T}}$ are within a single scaling window $\mathcal{O}(N^{-1/\nu})$. In addition to two correlation-length exponents ν_1 and ν_2 , other rich critical behaviors occur. In the broad scaling window $\mathcal{O}(N^{-1/\nu_2})$, the fractal dimensions are different from that in the narrow one $\mathcal{O}(N^{-1/\nu_1})$ including \mathcal{T}_N , and they are asymmetric at the two sides of the criticality. Moreover, at the super-critical side, the largest cluster and the others have different fractal dimensions.

In the conventional ensemble with a fixed density of occupied bonds, correct scaling predictions are difficult due to the sophisticated and anomalous phenomena. In contrast, the scaling behaviors in the event-based ensemble are rather clean and enable us to determine with a high precision the percolation threshold T_c and a variety of critical exponents in dimensions from 2 to 6 and on random graphs (Table I). As a result, a systematic comparison with the standard bond percolation becomes possible, and the explosive feature of the transition is clearly illustrated. Since multiple scalings may exist in other statistical systems, the event-based method can find wide ap-

TABLE I. Results of percolation threshold T_c and critical exponents with respect to system volume N . The systems are hypercubic lattice for finite dimension d and on random graph for $d = \infty$. The fractal dimensions d_f^\pm and $d_{f_2}^\pm$ are for the broad scaling window $\mathcal{T}_c^\pm(N, \nu_2)$.

d	T_c	Explosive percolation						Bond percolation [28–32]		
		$1/\nu_1$	$1/\nu_2$	d_f	d_f^-	d_f^+	$d_{f_2}^+$	T_c	$1/\nu$	d_f
2	1.053129(5)	0.512(1)	0.484(4)	0.979(1)	0.949(3)	0.980(3)	0.93(2)	1	3/8	91/96
3	0.966301(1)	0.595(8)	0.500(1)	0.924(5)	0.789(8)	0.943(3)	0.80(2)	0.746435	0.380	0.841
4	0.936642(2)	0.67(4)	0.501(2)	0.90(1)	0.705(3)	0.930(7)	0.70(1)	0.640525	0.365	0.761
5	0.923283(1)	0.71(3)	0.501(1)	0.915(5)	0.68(3)	0.93(2)	0.69(2)	0.590857	0.349	0.705
6	0.915853(1)	0.72(2)	0.499(2)	0.921(8)	0.66(2)	0.951(3)	0.70(4)	0.565210	1/3	2/3
∞	0.8884491(2)	0.740(2)	0.503(3)	0.935(1)	0.657(3)	0.956(2)	0.710(5)	1/2	1/3	2/3

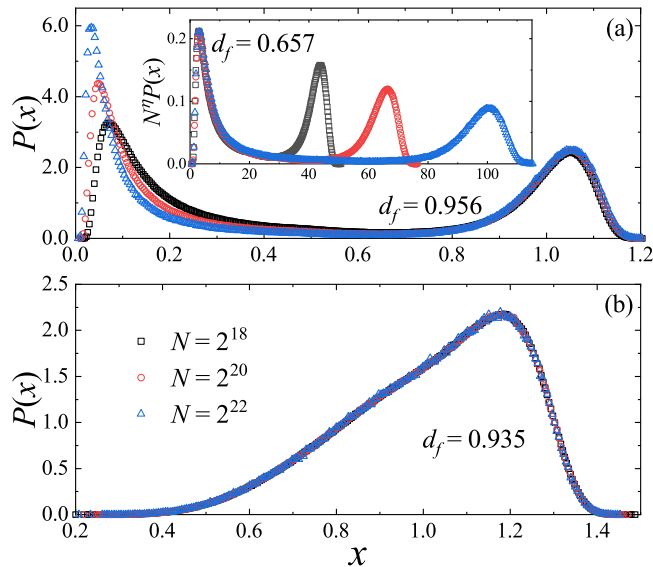


FIG. 1. Illustration of ensemble inequivalence by the largest-cluster probability distribution $P(x = C_1/N^{d_f})$ on random graphs, where the value of d_f is tuned to achieve data collapse for different volumes N . (a) is for the conventional ensemble at T_c and (b) is for the event-based ensemble at \mathcal{T}_N . The inset of (a) is for data collapse for the left hump, where the height is rescaled by factor N^η with $\eta = 0.08$.

plications.

Method and Observables.—By adopting the basic product rule and a flatten tree data structure, at each time step t we insert one of two randomly chosen bonds giving the smaller product of cluster sizes, and record the sizes of clusters as C_i ($i = 1, 2, \dots$) and the one-step increasing gap of the largest cluster $\Delta_C(t) \equiv C_1(t) - C_1(t-1)$. Roughly speaking, as t evolves, the gap Δ_C first increases in the sub-critical phase with small clusters, peaks near the percolation threshold, and finally decreases in the super-critical phase with a giant and dense cluster. The pseudo-critical point $\mathcal{T}_N = t_1/N$ corresponds to the time step t_1 of the event that Δ_C reaches its maximum. At \mathcal{T}_N , various observables are sampled, including the sizes of the largest and second largest clusters (C_1 and C_2), and the probability distribution $P(x = C_1)$. Their average values are calculated as T_N, C_1 and C_2 .

The thermodynamic threshold T_c is obtained by the least-

squares fit of the T_N data to

$$T_N = T_c + N^{-1/\nu_1}(a_0 + a_1 N^{-\omega_1} + a_2 N^{-\omega_2} + \dots), \quad (1)$$

where the terms with ω_i ($i = 1, 2$) account for finite-size corrections. The results are shown in Table I. For convenience, the critical exponents are quoted with respect to system volume N rather than linear size L .

Ensemble Inequivalence.—As an example of the anomalous behaviors in the conventional ensemble, we consider the probability distribution $P(x = C_1)$ at $T_c = 0.8884491$ for random graphs. It is clear that $P(x)$ exhibits a bimodal distribution (Fig. 1(a)). Different fractal dimensions are used to obtain data collapse for each hump, and the total probability for the left hump asymptotically vanishes with a small exponent. In contrast, Fig. 1(b) shows that, at the pseudo-critical point \mathcal{T}_N , $P(x)$ is unimodal and is well renormalized by a single fractal dimension. This provides solid evidence for the continuity of explosive percolation.

Moreover, neither of the two fractal dimensions in Fig. 1(a) is identical to the correct value $d_f = 0.935$ in Fig. 1(b). Since the normalized distribution $P(x = C_1/N^{d_f})$ holds true in the $N \rightarrow \infty$ limit, this inequivalence of two ensembles cannot vanish as N increases, and, thus, the d_f value cannot be correctly extracted from the conventional ensemble.

Two scaling windows.—The observed ensemble inequivalence is counter-intuitive and seems inconsistent with the standard finite-size scaling (FSS) theory. Let us recall some basic ideas. Near a critical point T_c , the diverging correlation length, $\xi(T) \sim |T - T_c|^{-\nu_L}$, is the only characteristic length scale (ν_L is the correlation-length exponent with respect to L), and the scaling of a physical quantity $Q(T)$ is then a function of ξ . The FSS theory assumes that, for a finite system, ξ_L is saturated to be the order of linear size L when approaching some pseudo-critical point T_N , and accordingly, the FSS of Q reads

$$Q(T, N) \sim N^y \tilde{Q}(N^{1/\nu}(T - T_c)), \quad (2)$$

where \tilde{Q} is a universal function, and $\nu/d = \nu_L$ and y are critical exponents. The pseudo-critical point is $T_N \approx T_c + aN^{-1/\nu}$ from $\xi_L \sim L$, with a some constant. Thus, the FSS of Q near T_N still follows Eq. (2), with the argument $(T - T_c)L^{1/\nu}$ in \tilde{Q} being shifted as $(T - T_N)N^{1/\nu} + a$. This means that the observed

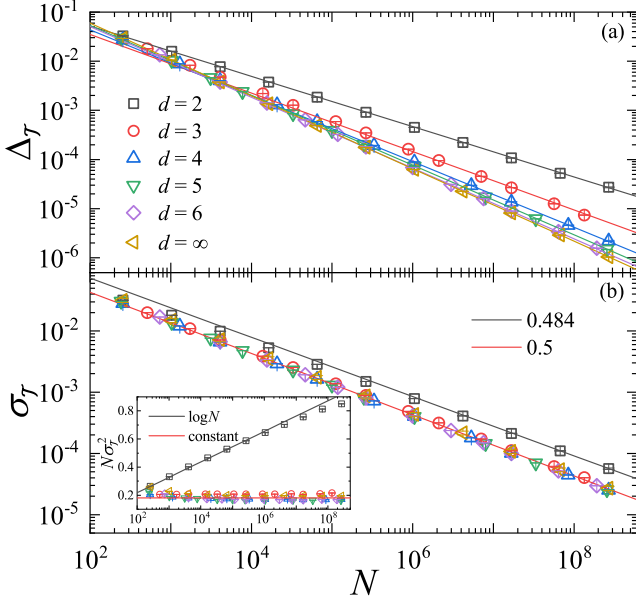


FIG. 2. Illustration of two scaling windows by the pseudo-critical distance $\Delta_{\mathcal{T}} \equiv \langle |\mathcal{T}_N - \mathcal{T}_{N,2}| \rangle$ (a) and the variance $\sigma_{\mathcal{T}}$. The exponent $1/\nu_2$ is consistent $1/2$ except for $d = 2$, while $1/\nu_1$ is d -dependent and larger than $1/2$. The inset of (b) shows the linear-log plot of the specific-heat-like quantity $N\sigma_{\mathcal{T}}^2$ as a function of system volume N .

ensemble equivalence should not be attributed to the deviation of T_N from T_c .

We now argue that the explosive percolation exhibits two scaling windows: while the deviation $T_N - T_c \sim N^{-1/\nu_1}$, the sample-to-sample fluctuation $\sigma_{\mathcal{T}}$ is of order $\mathcal{O}(N^{-1/\nu_2})$ with $\nu_2 > \nu_1$. As a result, the fluctuation plays an important role in the fixed-bond-density ensemble.

In actual simulations, a set of pseudo-critical points, $\mathcal{T}_{N,\ell}$ ($\ell = 1, 2, \dots$), is sampled from events that the gap Δ_C reaches its ℓ -th maximal value (\mathcal{T}_N is simply $\mathcal{T}_{N,1}$). The asymptotic behavior $T_{N,\ell} - T_c \sim N^{-1/\nu_1}$ is confirmed for all ℓ . To better estimate $1/\nu_1$, we fit the data of $\Delta_{\mathcal{T}} \equiv \langle |\mathcal{T}_N - \mathcal{T}_{N,2}| \rangle$ to

$$\Delta_{\mathcal{T}}(N) = N^{-1/\nu_1}(a_0 + a_1N^{-\omega_1} + a_2N^{-\omega_2} + \dots), \quad (3)$$

which significantly eliminates the sample-to-sample fluctuation. Also, the variance $\sigma_{\mathcal{T}}$ of \mathcal{T}_N is fitted to Eq. (3) with ν_1 being replaced by ν_2 . The results in Table I clearly support our argument of two scaling windows with $\nu_2 > \nu_1$, which is further illustrated by Fig. 2.

Unlike the d -dependent value of ν_1 , ν_2 is consistent with 2 for $d \geq 3$. According to the central-limit theorem, the distribution of an intensive quantity is of Gaussian type for sufficiently large N and its variance is of order $\mathcal{O}(N^{-1/2})$. As shown in the inset of Fig. 2(b), for $d \geq 3$ the specific-heat-like quantity $N\sigma_{\mathcal{T}}^2$ quickly converges to a constant as N increases, suggesting that the central-limit theorem might hold true. In two dimensions, since $1/\nu_1 = 0.512(1)$ is close to $1/\nu_2 = 0.484(4)$, we suspect that the small deviation $1/2 - 1/\nu_2 \approx 0.016$ is due to finite-size effects which are not adequately accounted for

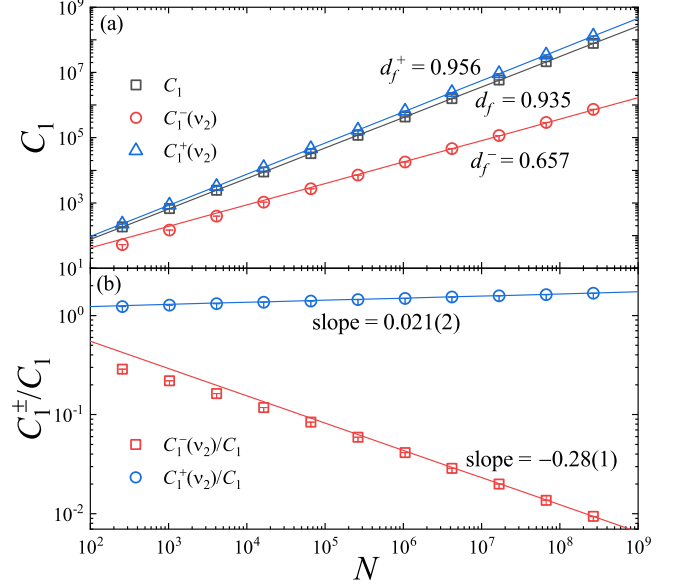


FIG. 3. Illustration of multiple fractal dimensions on random graphs by the largest-cluster size C_1 at \mathcal{T}_N and C_1^\pm at $\mathcal{T}_N^\pm(\nu_2) = \mathcal{T}_N \pm N^{-1/\nu_2}$. The ratios C_1^\pm/C_1 in (b) clearly show $d_f^\pm \neq d_f$.

in the fit. Indeed, Fig. 2(b) indicates that, as N increases, the slope of $\sigma_{\mathcal{T}}$ in log-scale increases toward $1/2$.

Multiple and fractal dimensions.— The C_1 and C_2 data at \mathcal{T}_N are well described by

$$C = N^{d_f}(a_0 + a_1N^{-\omega_1} + a_2N^{-\omega_2} + \dots), \quad (4)$$

and give a high-precision determination of the fractal dimension d_f for all dimensions (Table I). For each random Achlioptas process, we also sample $C_1^\pm(\nu_1)$ respectively at $\mathcal{T}_N^\pm(\nu_1) \equiv \mathcal{T}_N \pm aN^{-1/\nu_1}$ by simply taking $a = 1$. It is observed that, irrespective of dimension d , the $C_1^\pm(\nu_1)$ data are also well described by Eq. (4) and the d_f values are consistent with those in Table I. This means that, in the whole narrow scaling window $\mathcal{O}(N^{-1/\nu_1})$, the sample-to-sample fluctuation is suppressed and the scaling behaviors are rather clean. In contrast, it is difficult to obtain a reliable estimate of d_f in the conventional ensemble, as implied by Fig. 1(a) for random graphs, where the correct value $d_f = 0.935(1)$ cannot be extracted.

We then explore geometric properties within the broad scaling window $\mathcal{O}(N^{-1/\nu_2})$ by sampling at $\mathcal{T}_N^\pm(\nu_2) \equiv \mathcal{T}_N \pm N^{-1/\nu_2}$. While Eq. (4) can still describe the data of $C_1^\pm(\nu_2)$, the values of d_f^\pm are clearly different from those at \mathcal{T}_N (Table I). This implies the emergence of multiple fractal dimensions. On random graphs, the $C_1^\pm(\nu_2)$ data are shown in Fig. 3(a) and their ratios to $C_1(\mathcal{T}_N)$ are given in Fig. 3(b). The value $d_f^- = 0.657(3)$ at the sub-critical side explains the appearance of the left hump in Fig. 1(a), and $d_f^+ = 0.956(3)$ at the super-critical side agrees well with the right hump. In other words, in the conventional ensemble, the bimodal feature of $P(x)$ is solely from the broad scaling window $\mathcal{O}(N^{-1/\nu_2})$, and the cor-

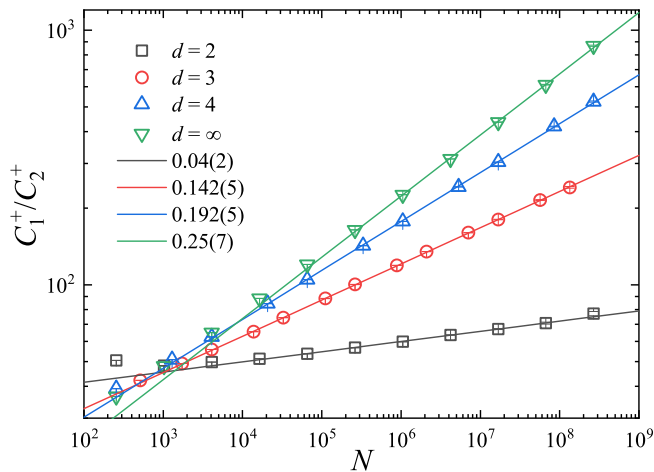


FIG. 4. Illustration of two length scales at $\mathcal{T}_N^+ = \mathcal{T}_N + N^{-1/\nu_2}$ by size ratio C_1^+/C_2^+ for the largest and the second largest cluster.

rect critical scaling at \mathcal{T}_N is hidden in the sophisticated mixing effects.

Asymmetric fractal dimensions.— Another important feature in Fig. 3 is that, in the broad window $O(N^{-1/\nu_2})$, the FSS of the largest cluster C_1 is asymmetric at the two sides of \mathcal{T}_N . Namely, the fractal dimensions, d_f^- and d_f^+ , take different values, irrespective of d (Table I).

We also sample size C_2^+ of the second largest cluster at $\mathcal{T}_N^+(\nu_2)$, and fit the C_2^+ data by Eq. (4). At sub-critical side, the fractal dimension $d_{f_2}^-$ is consistent with d_f^- for the largest cluster. However, at super-critical side, $d_{f_2}^+$ value is significantly smaller than d_f^+ (Table I). This means that, at $\mathcal{T}_N^+(\nu_2)$, the largest and the second largest cluster have different length scales, as illustrated by ratio C_1^+/C_2^+ in Fig. 4.

In fact, when the event-based sampling is taken at $\mathcal{T}_N^\pm(\nu)$ with exponent $\nu_1 < \nu < \nu_2$, the fractal dimensions, d_f^\pm and $d_{f_2}^\pm$, are found to continuously vary with exponent ν (see Supplemental Material). This gives further sophistication of scaling behaviors in the conventional ensemble.

Discussion and Outlook.— By an event-based method and extensive simulations, we find that the Achlioptas process for any d has two scaling windows: the distance of the average pseudo-critical point T_N from the percolation threshold T_c and the standard deviation of \mathcal{T}_N are characterized by two distinct exponents ν_1 and ν_2 . Based on numerical evidences, we assume that, at least for $d \geq 3$, the fluctuation of \mathcal{T}_N is of Gaussian type and thus $\nu_2 = 2$. Finite-size scaling (FSS) behaviors of quantities, sampled at the random point \mathcal{T}_N and its narrow scaling window $O(N^{-1/\nu_1})$, are rather clean and can be described by the standard FSS ansatz like Eqs. (1)-(4). As a result, we determine with a high precision the percolation threshold T_c and various critical exponents from $d = 2$ to 6 and on random graphs (Table I).

By a systematic comparison with the standard bond percolation (BP) model, we reveal the explosive but continuous nature of the explosive percolation (EP), especially for $d \geq 3$. In

two dimensions, $T_c(\text{EP}) \approx 1.053$ is slightly delayed about 5% of $T_c(\text{BP}) = 1$, and the fractal dimensions $d_f(\text{EP})$ and $d_f(\text{BP})$ are close to each other. Nevertheless, the explosive transition is clearly sharper as seen from exponent $1/\nu$. As d increases, the gap $T_c(\text{EP}) - T_c(\text{BP})$ becomes larger, and the explosive feature becomes clearer as reflected by the increasing value of $1/\nu_1$. Interestingly, it seems that $1/\nu$ for standard percolation reaches a maximum around $d = 3$, while d_f for explosive percolation has a minimum around $d = 4$.

Within the broad scaling window $O(N^{-1/\nu_2})$, rich phenomena are observed, including multiple and asymmetric fractal dimensions and two length scales at the super-critical side. Note that multiple scaling windows are also observed in the high-dimensional Ising model, which are interpreted as the simultaneous existence of multiple fixed points in the language of renormalization group [33–36]. However, a theoretical understanding is still needed for explosive percolation. A possible scenario is that, outside the narrow window $O(N^{-1/\nu_1})$, the rich behaviors are effectively the crossover phenomena from finite systems to thermodynamic limit. Even though, quantitative predictions are desired for the multiple fractal dimensions in Table I.

Our work is of practical importance. First of all, we point out that the anomalous phenomena, previously observed in the conventional ensemble of fixed bond density, are actually the mixing effects of multiple fractal structures. In particular, the bimodal probability distribution is not a sign of first-order phase transition but from the asymmetric scalings above and below \mathcal{T}_N . Second, we point out that, in the conventional ensemble, correct scaling predictions are difficult and reliable estimates of critical exponents are challenging. Finally, we point out that the event-based method can find broad applications. An immediate and important application is to address the controversial debate whether the explosive percolation universality should depend on the bond-inserting rules adopted in the Achlioptas process. Large sample-to-sample fluctuations can widely exist in systems like disordered ones [37, 38], it is certain that the event-based method can serve as a powerful tool in these cases. Further, even for usual equilibrium statistical systems, the event-based method has its own advantage by sampling the pseudo-critical point \mathcal{T}_N as some random event. In contrast, in traditional simulations, T_N is frequently defined as the peak position of susceptibility or specific heat, and the location of T_N needs a large number of samples and suffers from the intrinsic mathematical difficulty of finding a maximum point.

The research was supported by the Science and Technology Committee of Shanghai (Grant No. 20DZ2210100), the National Key R&D Program of China (Grant No. 2018YFA0306501).

* lim@hfut.edu.cn

† yjdeng@ustc.edu.cn

- [1] D. Stauffer and A. Aharony, *Introduction to percolation theory*, 2nd ed. (Taylor & Francis, London, 1991).
- [2] D. J. Jacobs and M. F. Thorpe, Generic rigidity percolation: The pebble game, *Phys. Rev. Lett.* **75**, 4051 (1995).
- [3] D. J. Jacobs and M. F. Thorpe, Generic rigidity percolation in two dimensions, *Phys. Rev. E* **53**, 3682 (1996).
- [4] P. Grassberger, Directed percolation in 2+1 dimensions, *J. Phys. A: Math. Gen.* **22**, 3673 (1989).
- [5] J. Wang, Z. Zhou, Q. Liu, T. M. Garoni, and Y. Deng, High-precision monte carlo study of directed percolation in $(d + 1)$ dimensions, *Phys. Rev. E* **88**, 042102 (2013).
- [6] S. Boccaletti, J. Almendral, S. Guan, I. Leyva, Z. Liu, I. Sendiña-Nadal, Z. Wang, and Y. Zou, Explosive transitions in complex networks' structure and dynamics: Percolation and synchronization, *Phys. Rep.* **660**, 1 (2016).
- [7] D. Achlioptas, R. M. D'Souza, and J. Spencer, Explosive percolation in random networks, *Science* **323**, 1453 (2009).
- [8] R. M. Ziff, Explosive growth in biased dynamic percolation on two-dimensional regular lattice networks, *Phys. Rev. Lett.* **103**, 045701 (2009).
- [9] R. M. Ziff, Scaling behavior of explosive percolation on the square lattice, *Phys. Rev. E* **82**, 051105 (2010).
- [10] Y. S. Cho, J. S. Kim, J. Park, B. Kahng, and D. Kim, Percolation transitions in scale-free networks under the achlioptas process, *Phys. Rev. Lett.* **103**, 135702 (2009).
- [11] F. Radicchi and S. Fortunato, Explosive percolation in scale-free networks, *Phys. Rev. Lett.* **103**, 168701 (2009).
- [12] E. J. Friedman and A. S. Landsberg, Construction and analysis of random networks with explosive percolation, *Phys. Rev. Lett.* **103**, 255701 (2009).
- [13] R. A. da Costa, S. N. Dorogovtsev, A. V. Goltsev, and J. F. F. Mendes, Explosive percolation transition is actually continuous, *Phys. Rev. Lett.* **105**, 255701 (2010).
- [14] R. M. D'Souza and M. Mitzenmacher, Local cluster aggregation models of explosive percolation, *Phys. Rev. Lett.* **104**, 195702 (2010).
- [15] J. Nagler, A. Levina, and M. Timme, Impact of single links in competitive percolation, *Nat. Phys.* **7**, 265 (2011).
- [16] O. Riordan and L. Warnke, Achlioptas processes are not always self-averaging, *Phys. Rev. E* **86**, 011129 (2012).
- [17] P. Grassberger, C. Christensen, G. Bizhani, S.-W. Son, and M. Paczuski, Explosive percolation is continuous, but with unusual finite size behavior, *Phys. Rev. Lett.* **106**, 225701 (2011).
- [18] L. Tian and D.-N. Shi, The nature of explosive percolation phase transition, *Phys. Lett. A* **376**, 286 (2012).
- [19] N. Bastas, K. Kosmidis, and P. Argyrakis, Explosive site percolation and finite-size hysteresis, *Phys. Rev. E* **84**, 066112 (2011).
- [20] F. Radicchi and S. Fortunato, Explosive percolation: A numerical analysis, *Phys. Rev. E* **81**, 036110 (2010).
- [21] Y. S. Cho and B. Kahng, Suppression effect on explosive percolation, *Phys. Rev. Lett.* **107**, 275703 (2011).
- [22] H. K. Lee, B. J. Kim, and H. Park, Continuity of the explosive percolation transition, *Phys. Rev. E* **84**, 020101 (2011).
- [23] O. Riordan and L. Warnke, Explosive percolation is continuous, *Science* **333**, 322 (2011).
- [24] R. M. D'Souza and J. Nagler, Anomalous critical and supercritical phenomena in explosive percolation, *Nat. Phys.* **11**, 531 (2015).
- [25] N. A. M. Araújo and H. J. Herrmann, Explosive percolation via control of the largest cluster, *Phys. Rev. Lett.* **105**, 035701 (2010).
- [26] W. Chen and R. M. D'Souza, Explosive percolation with multiple giant components, *Phys. Rev. Lett.* **106**, 115701 (2011).
- [27] J. Fan, J. Meng, Y. Liu, A. A. Saberi, J. Kurths, and J. Nagler, Universal gap scaling in percolation, *Nat. Phys.* **16**, 455 (2020).
- [28] G. Paul, R. M. Ziff, and H. E. Stanley, Percolation threshold, fisher exponent, and shortest path exponent for four and five dimensions, *Phys. Rev. E* **64**, 026115 (2001).
- [29] J. Wang, Z. Zhou, W. Zhang, T. M. Garoni, and Y. Deng, Bond and site percolation in three dimensions, *Phys. Rev. E* **87**, 052107 (2013).
- [30] X. Xu, J. Wang, J.-P. Lv, and Y. Deng, Simultaneous analysis of three-dimensional percolation models, *Front. Phys.* **9**, 113 (2013).
- [31] S. Mertens and C. Moore, Percolation thresholds and fisher exponents in hypercubic lattices, *Phys. Rev. E* **98**, 022120 (2018).
- [32] Z. Zhang, P. Hou, S. Fang, H. Hu, and Y. Deng, Critical exponents and universal excess cluster number of percolation in four and five dimensions, *Physica A* **580**, 126124 (2021).
- [33] M. Wittmann and A. P. Young, Finite-size scaling above the upper critical dimension, *Phys. Rev. E* **90**, 062137 (2014).
- [34] Z. Zhou, J. Grimm, S. Fang, Y. Deng, and T. M. Garoni, Random-length random walks and finite-size scaling in high dimensions, *Phys. Rev. Lett.* **121**, 185701 (2018).
- [35] S. Fang, Z. Zhou, and Y. Deng, Percolation effects in the fortuin-kasteleyn ising model on the complete graph, *Phys. Rev. E* **103**, 012102 (2021).
- [36] S. Fang, Z. Zhou, and Y. Deng, Geometric upper critical dimensions of the ising model, *Chin. Phys. Lett.* **39**, 080502 (2022).
- [37] F. Pázmándi, R. T. Scalettar, and G. T. Zimányi, Revisiting the theory of finite size scaling in disordered systems: ν can be less than $2/d$, *Phys. Rev. Lett.* **79**, 5130 (1997).
- [38] K. Bernardet, F. Pázmándi, and G. G. Batrouni, Disorder averaging and finite-size scaling, *Phys. Rev. Lett.* **84**, 4477 (2000).

Supplemental Material for “Multiple and asymmetric scalings in explosive percolation”

Scalings at $\mathcal{T}_{N,\ell}$ for different ℓ

As stated in the main text, the pseudo-critical point $\mathcal{T}_{N,\ell}$ can be defined by the event that the one-step increasing gap of the largest cluster Δ_C reaches its ℓ -th maximal value. All the averages $T_{N,\ell} \equiv \langle \mathcal{T}_{N,\ell} \rangle$ for different ℓ satisfy the same finite-size scaling

$$T_{N,\ell} = T_c + N^{-1/\nu_1} (a_0 + a_1 N^{-\omega_1} + a_2 N^{-\omega_2} + \dots).$$

From Fig. S1 (a), we can find that the pseudo-critical point $T_{N,\ell}$ for different ℓ approaches to the critical point T_c from different directions, i.e., a_0 can be either positive or negative. Figure S1 (b) shows that the distance between two pseudo-critical points $\Delta_{\mathcal{T},\ell} \equiv |\mathcal{T}_{N,\ell} - \mathcal{T}_{N,\ell+1}|$ displays an ℓ -independent scaling. This further provides an evidence that the asymptotic behaviors of all the pseudo-critical points $T_{N,\ell}$ give the same scaling exponent $1/\nu_1$, but different a_0 and correction terms.

In our experience, the statistical error of the observable at $\mathcal{T}_{N,\ell}$ increases with ℓ . This is mainly because $\mathcal{T}_{N,\ell}$ for $\ell > 1$ can be located either below or above the criticality, where the observable could be very different. A direct evidence is the bimodal distribution of C_1 at $\mathcal{T}_{N,\ell}$ for $\ell > 1$, see Fig. S1 (c). A brutal average on these remarkably different observables certainly introduces a large statistical error. Thus, it is not a good choice to use the Monte Carlo data at $\mathcal{T}_{N,\ell}$ with a large ℓ .

In fact, the distribution of C_1 at $\mathcal{T}_{N,1}$ is not a clean unimodal distribution yet. As shown in Fig. S1 (c), it is clear that the distribution is not symmetric on the two sides of the peak. This indicates that more than one case could be involved at $\mathcal{T}_{N,1}$. We can use the relationship between $\mathcal{T}_{N,1}$ and $\mathcal{T}_{N,2}$ to divide the samples into two groups, i.e., $\mathcal{T}_{N,1} > \mathcal{T}_{N,2}$ and $\mathcal{T}_{N,1} < \mathcal{T}_{N,2}$. Then, the symmetric unimodal distribution of C_1 can be found in both the two groups.

Different from the bimodal distribution at the critical point T_c (see Fig. 1 in the main text), the bimodal distribution of Fig. S1 (c) only shows a unique fractal dimension $d_f = 0.935$. This is because all these pseudo-critical points $\mathcal{T}_{N,\ell}$ are located inside the narrow scaling window $\mathcal{O}(N^{-1/\nu_1})$.

The reordered pseudo-critical point $\mathcal{T}'_{N,\ell}$

To eliminate the bimodal distribution of observables at the pseudo-critical point $\mathcal{T}_{N,\ell}$, one can sort the pseudo-critical points $\mathcal{T}_{N,\ell}$ obtained in a single realization by their values before the statistics of observables. Specifically, in a single realization we can relabel the largest pseudo-critical point as $\mathcal{T}'_{N,1}$, the second largest one as $\mathcal{T}'_{N,2}$, and so on. Then, the statistics of observables can be done at these reordered pseudo-critical points $\mathcal{T}'_{N,\ell}$ over different realizations. Note that the result also depends on the total number of the pseudo-critical points used in the reorder process.

In Fig. S2, we can find that the distributions of C_1 for large and small ℓ become unimodal as expected. For a modest ℓ , this reorder process cannot guarantee that the pseudo-critical point $\mathcal{T}'_{N,\ell}$ is always larger or smaller than the critical point, which results in a bimodal distribution. For a better result, one can sort more pseudo-critical points in the reorder process. Since this reorder process just performs a linear recombination of the observables found at $\mathcal{T}_{N,\ell}$, thus it does not change the scaling behavior, see Fig. S2. In our experience, we cannot achieve a significantly improved fit result at the reordered pseudo-critical point $\mathcal{T}'_{N,\ell}$ for most cases. However, the reordered pseudo-critical point also has its advantages in dealing with some special cases, such as distinguishing the pseudo-critical points below and above the criticality.

The asymptotic behavior of T_N in different dimensions

In Fig. S3, we show the asymptotic behavior of $T_N \equiv \langle \mathcal{T}_N \rangle$ for different dimensions. We can see that for $d < 4$, the pseudo-critical point T_N approaches to T_c from below, while for $d > 4$, the pseudo-critical point T_N approaches to T_c from above. For $d = 4$, when the system is large enough, T_N will be also larger than T_c .

For the reordered pseudo-critical point $T'_{N,\ell}$, similar phenomenon can also be observed, see Fig. S4. We can find that $T'_{N,2}$ is always smaller than T_c , while $T'_{N,1}$ will be larger than T_c for $d \geq 4$. It should be noted that if we sort more pseudo-critical points, it is possible to find a $T'_{N,2}$ larger than T_c even for $d < 4$.

Fractal dimensions $d_f^\pm(\nu)$ for different ν

To explore geometric properties within different scaling windows, we sample observables at $\mathcal{T}_N^\pm(\nu) \equiv \mathcal{T}_N \pm N^{1/\nu}$. Note that this is also an event-based sampling, since $\mathcal{T}_N^\pm(\nu)$ is also dependent on the occurrence of a special event. In order to realize this

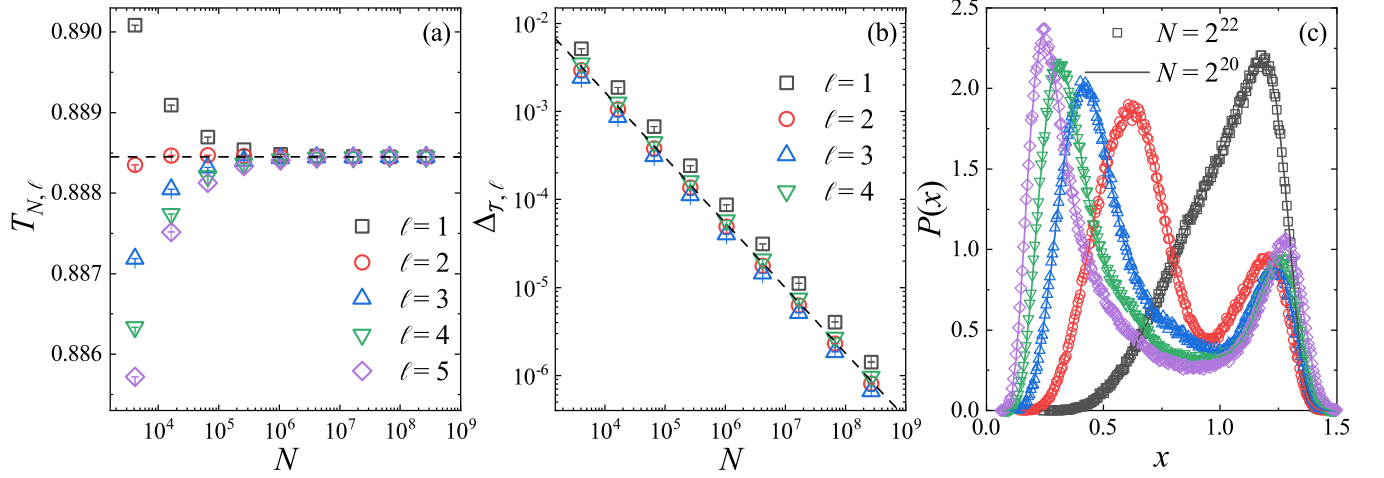


FIG. S1. (a) The pseudo-critical point $\mathcal{T}_{N,\ell}$ as a function of the system volume N for different ℓ . The black dashed line indicates the critical point $T_c = 0.8884491$. (b) The distance between two pseudo-critical points $\Delta_{\mathcal{T},\ell} \equiv \langle |\mathcal{T}_{N,\ell} - \mathcal{T}_{N,\ell+1}| \rangle$ as a function of the system volume N for different ℓ . The dashed line shows a power law with a negative slope $-1/\nu_1 = -0.74$. (c) The probability distribution of C_1 at pseudo-critical point $\mathcal{T}_{N,\ell}$ for different ℓ . Here $P(x)$ is the probability density function of $x = C_1/N^{d_f}$ with $d_f = 0.935$. The lines and scatters are for the systems of volumes $N = 2^{20}$ and $N = 2^{22}$, respectively. Here, the system is random graph.

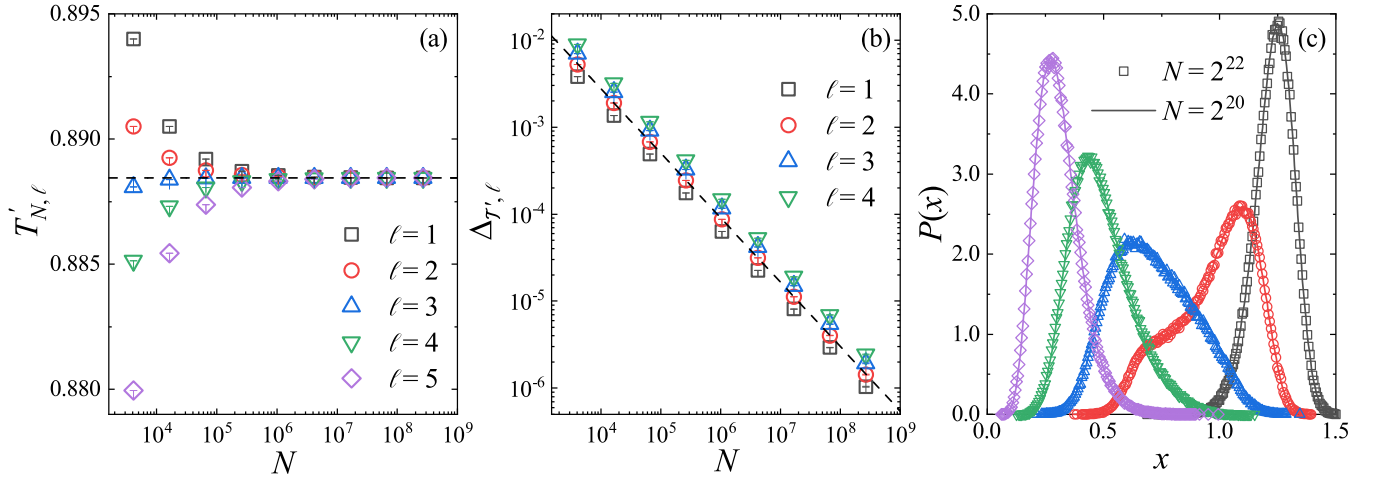


FIG. S2. (a) The reordered pseudo-critical point $\mathcal{T}'_{N,\ell}$ as a function of the system volume N for different ℓ . The black dashed line indicates the critical point $T_c = 0.8884491$. (b) The distance of two reordered pseudo-critical points $\Delta_{\mathcal{T}',\ell} \equiv \langle |\mathcal{T}'_{N,\ell} - \mathcal{T}'_{N,\ell+1}| \rangle$ as a function of the system volume N for different ℓ . The dashed line shows a power law with a negative slope $-1/\nu_1 = -0.74$. (c) The probability distribution of C_1 at reordered pseudo-critical point $\mathcal{T}'_{N,\ell}$ for different ℓ . Here $P(x)$ is the probability density function of $x = C_1/N^{d_f}$ with $d_f = 0.935$. The lines and scatters are for the systems of volumes $N = 2^{20}$ and $N = 2^{22}$, respectively. Here, the system is random graph.

sampling, we first identify the pseudo-critical point \mathcal{T}_N in a realization, and record the order in which bonds are occupied. Then, with the recorded bond sequence, one can reconstruct the percolation configurations at $\mathcal{T}_N^\pm(\nu)$. In this way, any observables at $\mathcal{T}_N^\pm(\nu)$ can be also obtained.

$$\nu = \nu_2$$

In Fig. S5, we show C_1 and $C_1^\pm(\nu_2)$ obtained by the event-based sampling as a function of the system volume N . We can find that C_1 and $C_1^\pm(\nu_2)$ show different fractal dimensions, indicating that there exists different fractal structures in the two scaling windows. In addition to Fig. 3 in the main text, we also show the multiple fractal dimensions of 3-dimensional systems in Fig. S6.

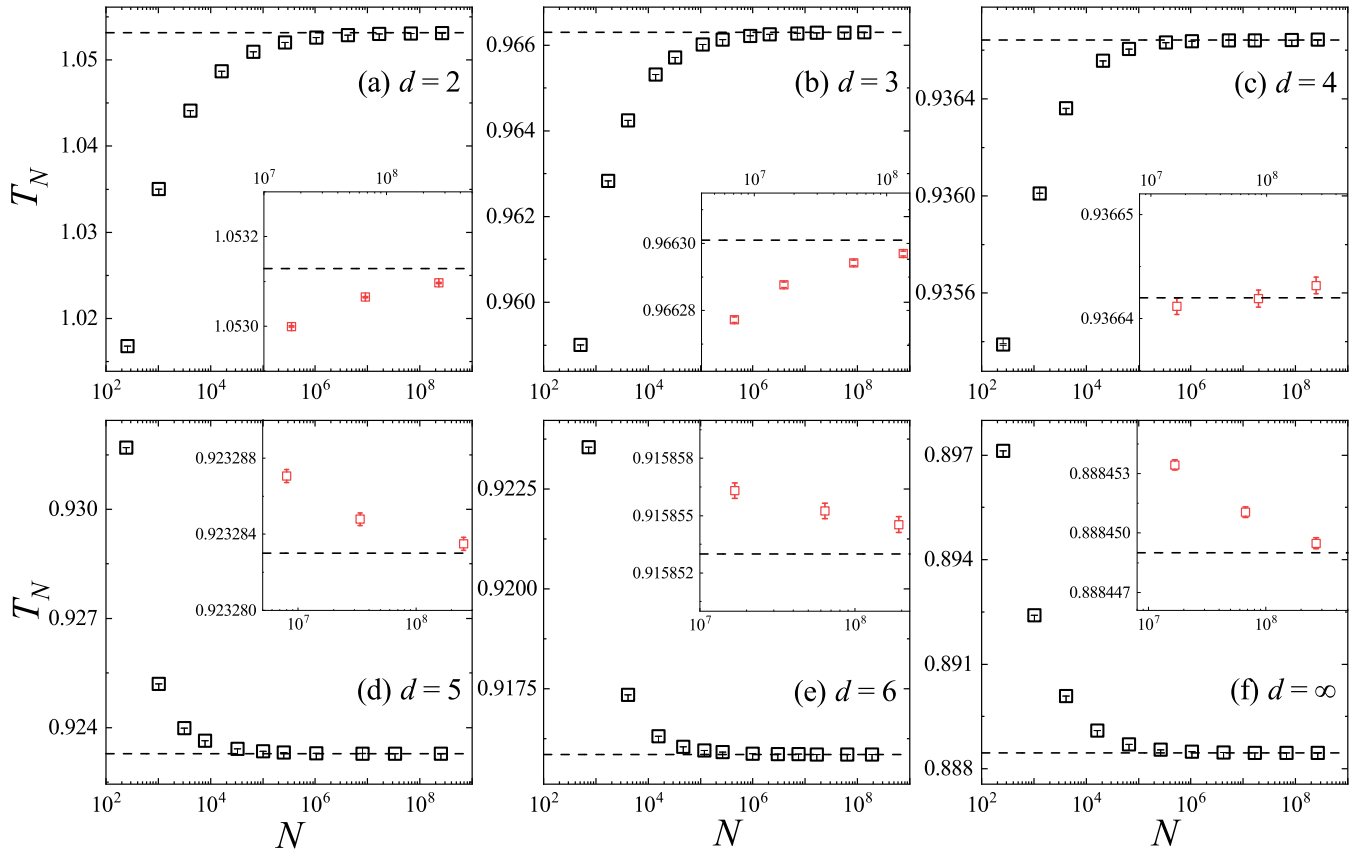


FIG. S3. The asymptotic behavior of the pseudo-critical point T_N in different dimensions. The insets show the zooming figures for large systems. The dashed lines show the corresponding critical point T_c .

$$\nu_1 < \nu < \nu_2$$

In Fig. S7, the ratios $C_1^\pm(\nu = 5/3)/C_1^\pm(\nu_2)$ are plotted as a function of the system volume N . We can find that both the two ratios scale in a power law with the increase of the system volume. This means that at $\mathcal{T}_N^\pm(\nu = 5/3)$ the largest cluster has a fractal dimension different from that at $\mathcal{T}_N^\pm(\nu_2)$. Similar phenomenon can also be found for other ν . In that, we conjecture that outside the narrow scaling window $\mathcal{O}(N^{-1/\nu_1})$, there exists continuously variable fractal dimensions $d_f^\pm(\nu)$.

Cluster size distribution

In Fig. S8, we show the cluster size distributions n_s at \mathcal{T}_c and $\mathcal{T}_c^\pm(\nu_2)$ on random graphs. We can find that all the three cases show the same Fisher exponent $\tau = 2.07$, which can be obtained by the hyperscaling relation $\tau = 1 + 1/d_f$ with $d_f = 0.935$. Moreover, different d_f are required to show a good data collapse for the power-law decay part, see Figs. S8 (d)-(f). Even so, at $\mathcal{T}_c^\pm(\nu_2)$ (Figs. S8 (e) and (f)) we cannot find a single fractal dimension that can show a good data collapse over the entire range of the distribution n_s as that at \mathcal{T}_c (Fig. S8 (d)). This is mainly due to the multiple fractal dimensions outside the narrow scaling window $\mathcal{O}(N^{-1/\nu_1})$. Similar phenomenon can also be observed at T_c shown in Fig. S9.

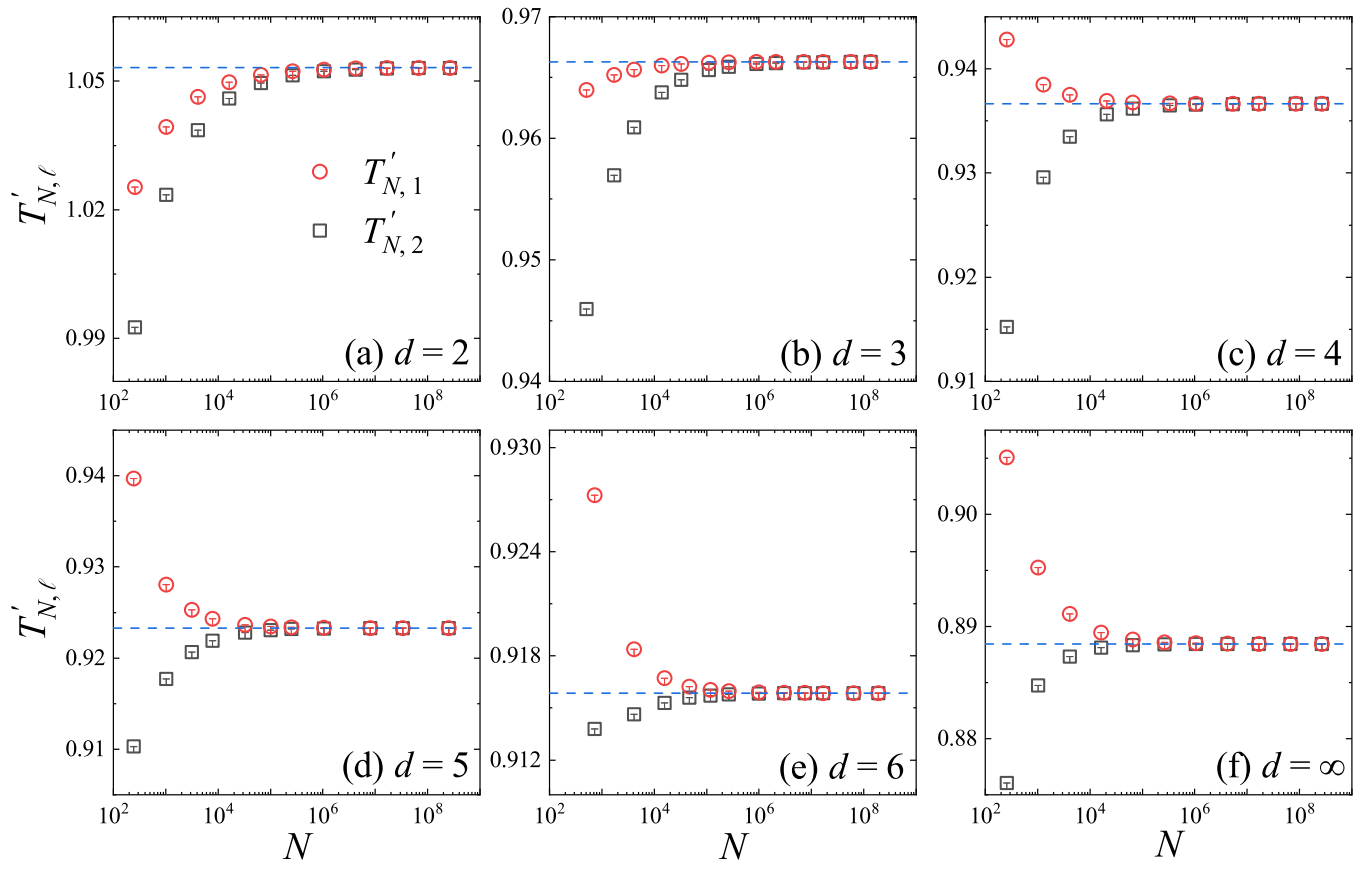


FIG. S4. The asymptotic behaviors of the reordered pseudo-critical points $T'_{N,1}$ and $T'_{N,2}$ in different dimensions. The dashed lines show the corresponding critical point T_c .

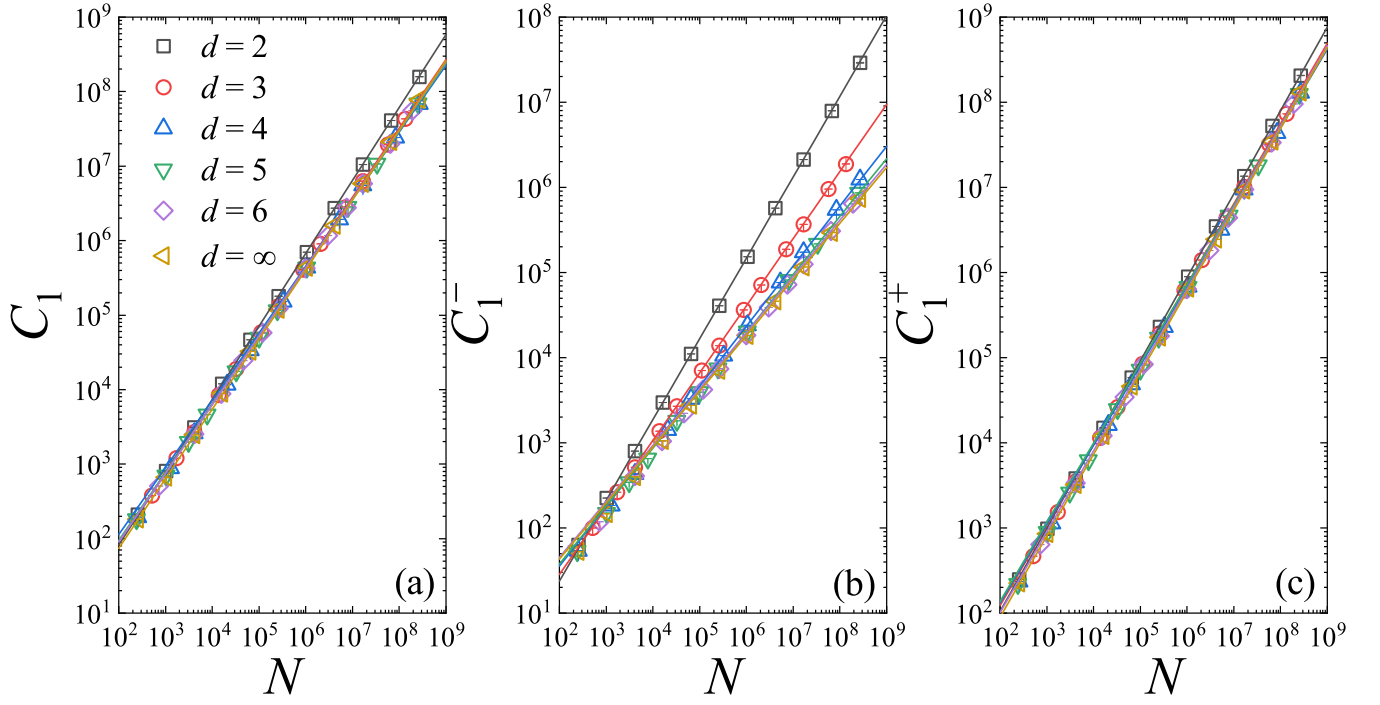


FIG. S5. The sizes of the largest clusters C_1 and $C_1^\pm(v_2)$ obtained by the event-based sampling as a function of the system volume N . The lines correspond to the fractal dimensions d_f and $d_f^\pm(v_2)$ shown in Table I of the main text.

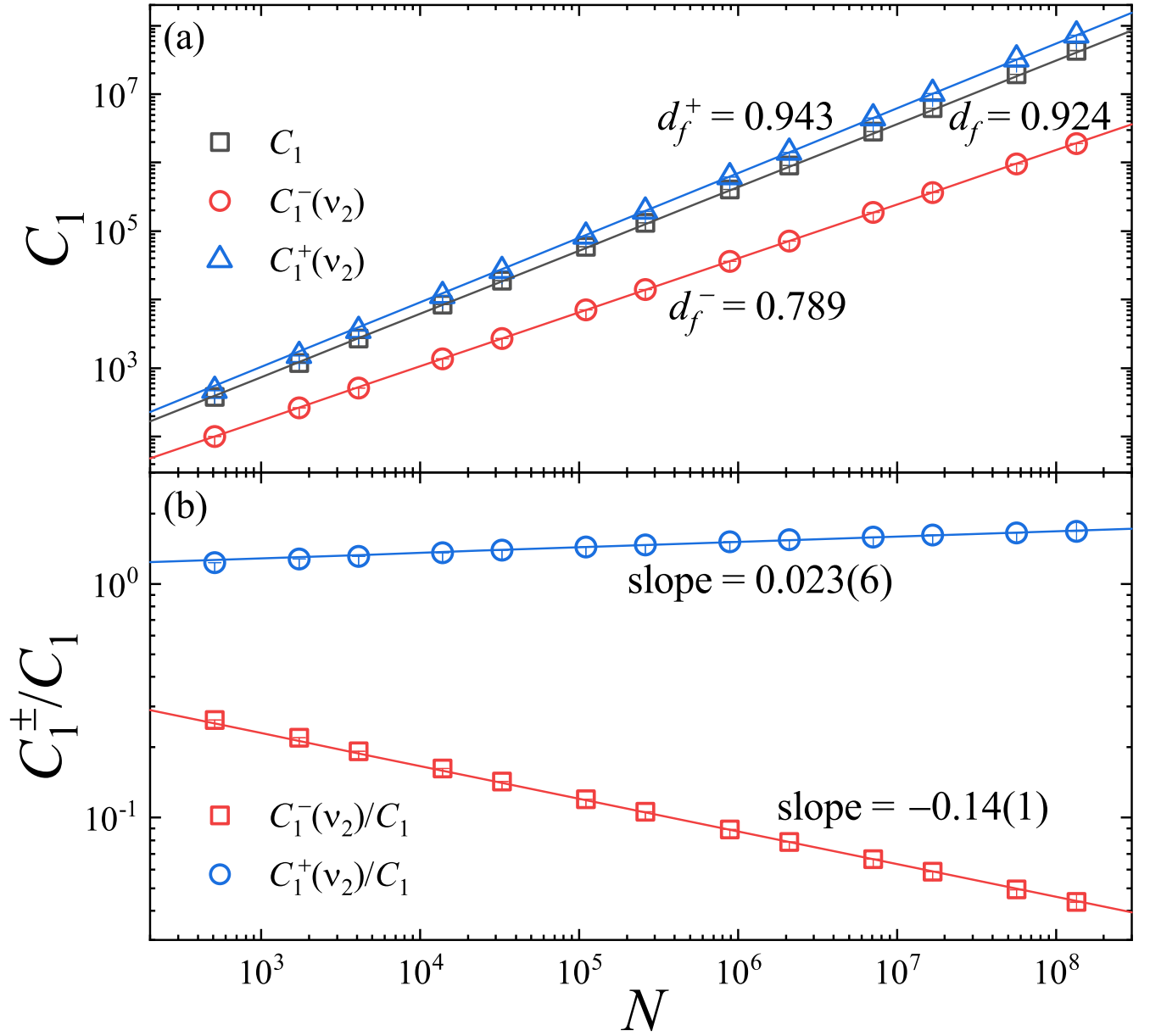


FIG. S6. Illustration of multiple fractal dimensions in dimension 3 by the largest-cluster size C_1 at \mathcal{T}_N and C_1^\pm at $\mathcal{T}_N^\pm(v_2)$. The ratios C_1^\pm/C_1 in (b) clearly show $d_f^\pm \neq d_f$.

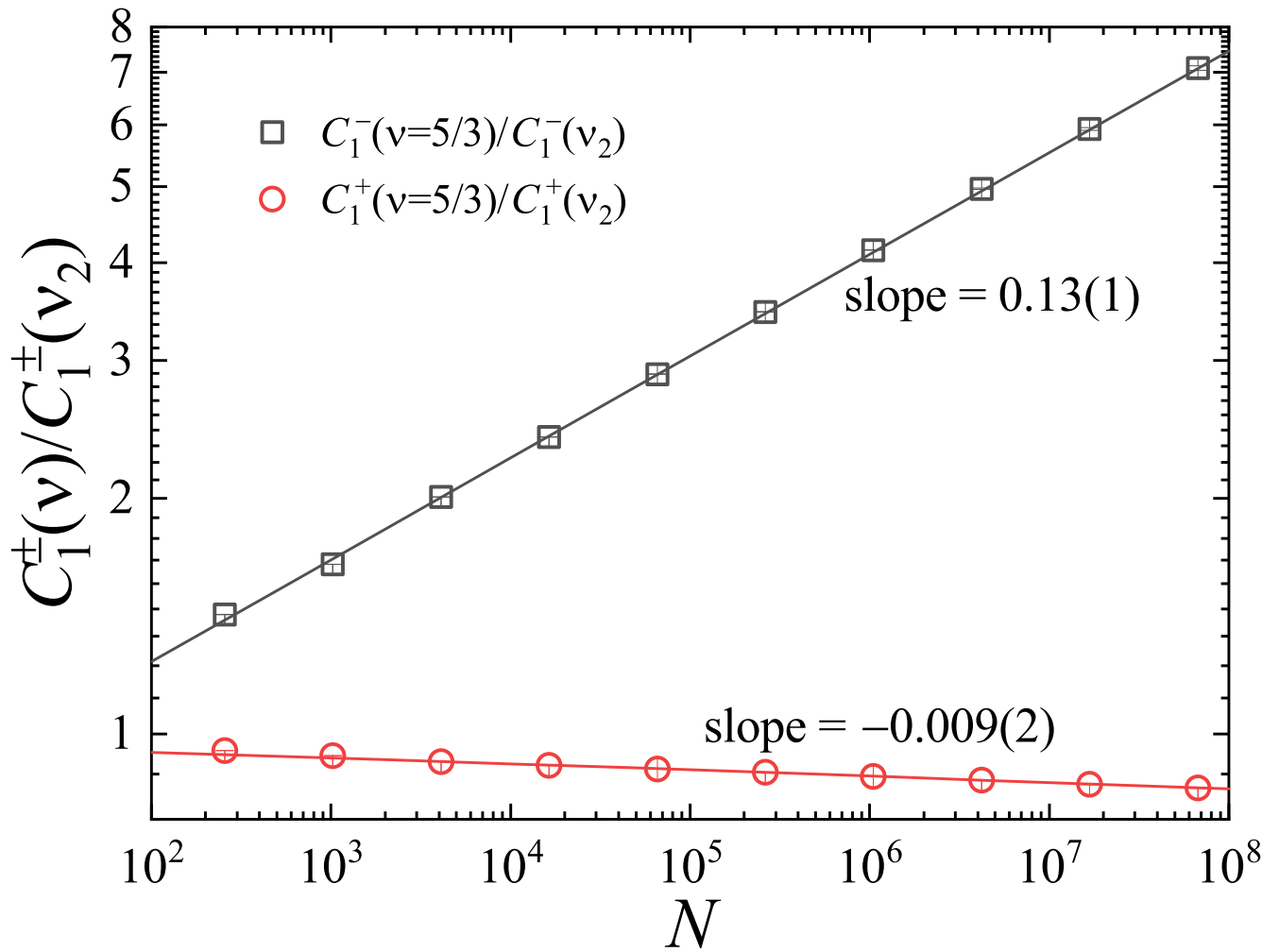


FIG. S7. The ratios $C_1^\pm(\nu = 5/3)/C_1^\pm(\nu_2)$ as a function of the system volume N on random graphs.

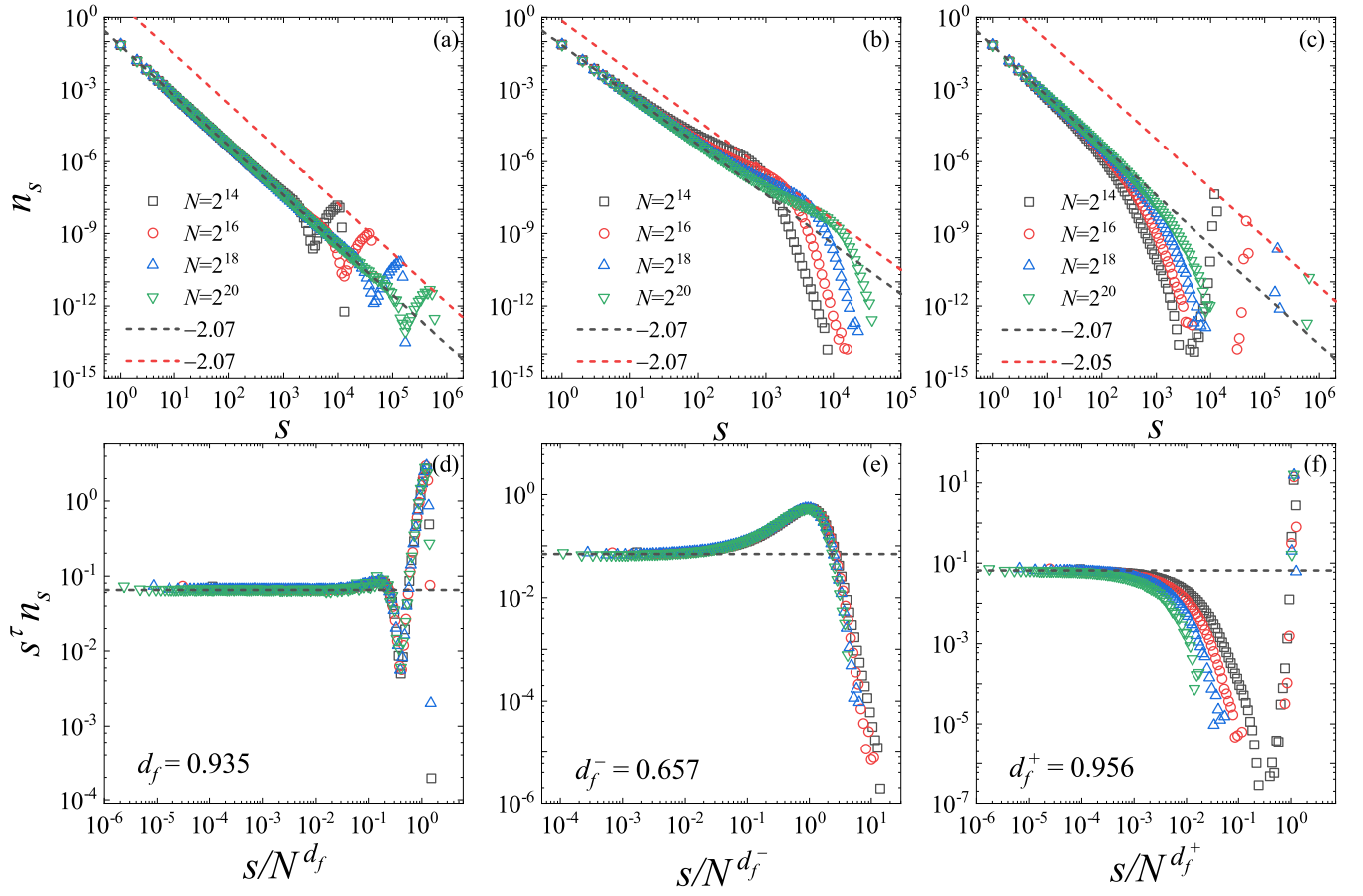


FIG. S8. The cluster size distributions n_s on random graphs at (a) \mathcal{T}_N , (b) $\mathcal{T}_N^-(\nu_2)$, and (c) $\mathcal{T}_N^+(\nu_2)$. With the hyperscaling relation $\tau = 1 + 1/d_f$, we know that $d_f = 0.935$ and $d_f^+ = 0.956$ corresponds to $\tau = 2.07$ and 2.05 , respectively. Sub-figures (d)-(f) are the corresponding rescaled forms of sub-figures (a)-(c) with $\tau = 2.07$, respectively.

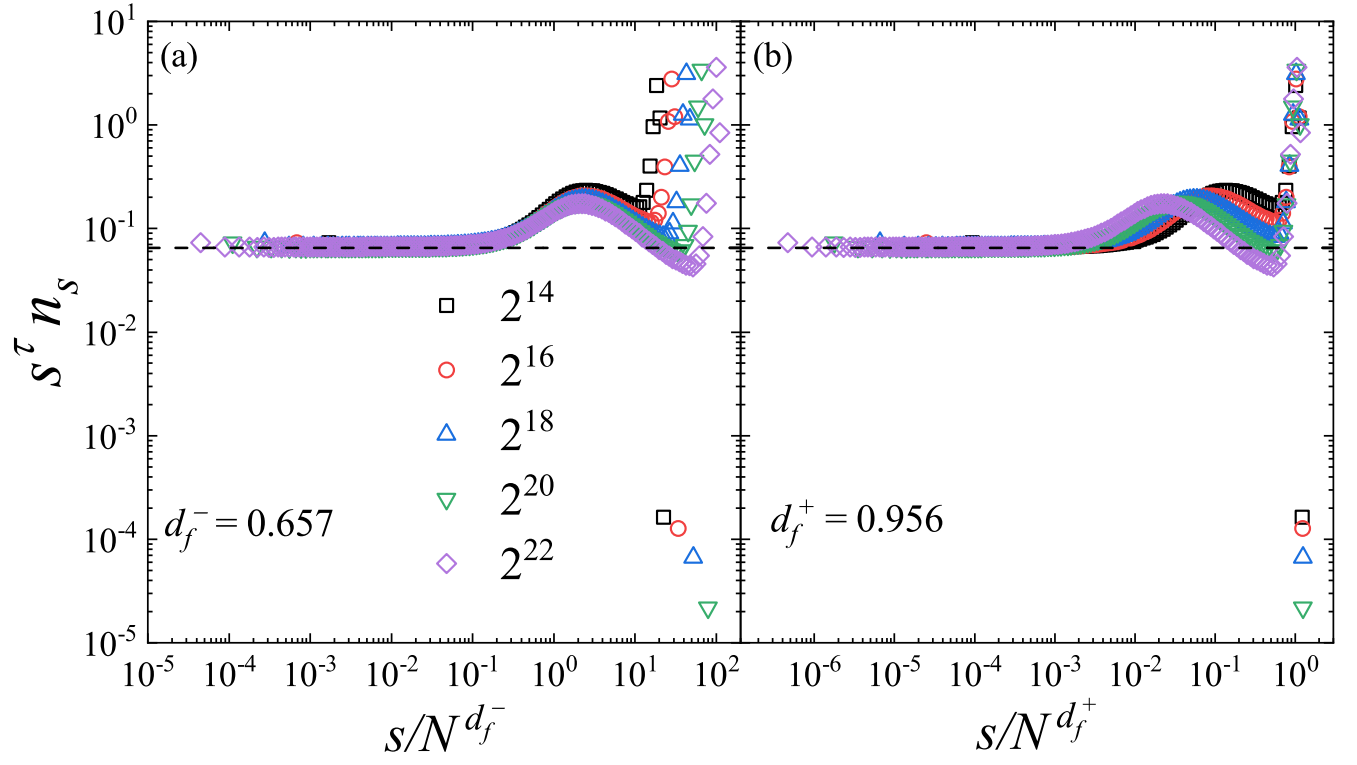


FIG. S9. The critical cluster size distribution n_s on random graphs at $T_c = 0.8884491$. Here, the Fisher exponent $\tau = 1 + 1/d_f = 1 + 1/0.935 = 2.07$ is used to rescale the cluster size distribution n_s .